REMCOM® Electromagnetic Simulation Software

Technical Report: Simulation of Plasma Materials in XFdtd

Validation examples comparing FDTD computational results to analytic solutions for complex plasma structures.

Technical Report: Simulation of Plasma Materials in XFdtd

1. Introduction

Plasmas are comprised of a medium of charged particles, ions, and electrons and are one of the most common forms of matter in the universe. Although plasmas generally exist in stars and clouds in space, they can be created by heating or applying a strong electromagnetic field to a neutral gas. High heat or pressure can strip electrons from atoms, creating positively charged ions and free electrons in an electrically-conducting medium, such as a plasma.

Of current interest is the formation and behavior of plasmas created by hypersonic vehicles passing through the atmosphere. These vehicles leave behind a plasma trail which can interfere with electromagnetic signals due to the conducting nature of the material. This presents interesting challenges both for radar detection of these vehicles and for radio communication and guidance through the plasma layer.

This paper discusses the finite-difference, time-domain (FDTD) method to simulate the behavior of plasma materials. There has been extensive work in this area in the past using FDTD, but most relevant to this application are approaches developed by Luebbers et. al. for the simulation of frequency-dependent materials in general [1], and plasmas specifically [2]. Further work on higher order dispersive materials [3] and magnetized plasma [4] further validated the approach. The technique was applied to three-dimensional, full-wave scattering from frequency-dependent materials in the 1993 Schelkunoff Best Paper Award publication in the IEEE Transactions on Antennas and Propagation [5]. These developments and future refinements are incorporated into Remcom's XFdtd® 3D Electromagnetic Simulation solver, which will be used to provide some of the results in this paper.

The simulation of plasmas will be discussed here starting with an explanation of the frequency-dependent model used, followed by validation of the method in one- and three-dimensions. In three dimensions, both monostatic and bistatic radar cross section results will be presented for validation.

2. The Debye-Drude Material Model Applied to Lossy Plasmas

The Debye-Drude material model describes a frequency varying relative permittivity function that includes loss and is a good fit for the complex permittivity of a lossy plasma. The Debye-Drude equation with one first order pole is

$$\varepsilon_r(\omega) = \epsilon_\infty + \frac{\epsilon_s - \epsilon_\infty}{1 + j\omega\tau_0} + \frac{\sigma}{j\omega\varepsilon_0}$$

where ε_∞ is the infinite frequency relative permittivity, ε_s is the static frequency relative permittivity, τ_0 is the relaxation time (in seconds), and σ is the electrical conductivity (Siemens/meter).

In comparison, the well-known frequency dependent relative complex dielectric constant for plasma is

$$\varepsilon_r(\omega) = \left(1 + \frac{\omega_p^2}{j\omega(f_c + j\omega)}\right)$$

where ω_p is the plasma frequency (Radians), and f_c is the collision frequency of the plasma (Hertz). This expression can be rearranged to put it in the same form as the Debye-Drude equation as

$$\varepsilon_r(\omega) = 1 - \frac{\frac{\omega_p^2}{f_c^2}}{1 + j\frac{\omega}{f_c}} + \frac{\omega_p^2}{j\omega f_c}$$

Comparing the two expressions results in the following equations:

$$\epsilon_s - \epsilon_\infty = -\frac{\omega_p^2}{f_c^2} \qquad \epsilon_\infty = 1 \qquad \tau_0 = \frac{1}{f_c}$$

The conductivity term is then

$$\sigma = \frac{\varepsilon_0 \omega_p^2}{f_c}$$

Consider the plasma discussed in [5] which had parameters of Plasma Frequency = 28.7 GHz, Collision Frequency = 20 GHz, the Debye-Drude parameters would be Infinite Frequency relative permittivity = 1, Static Frequency relative permittivity = -80.295, relaxation time = 5×10^{-11} sec, and conductivity = 14.397 S/m. The complex permittivity of this model may be plotted as real and imaginary parts shown in Figure 1. This plasma model and parameters will be used for future examples in this paper.

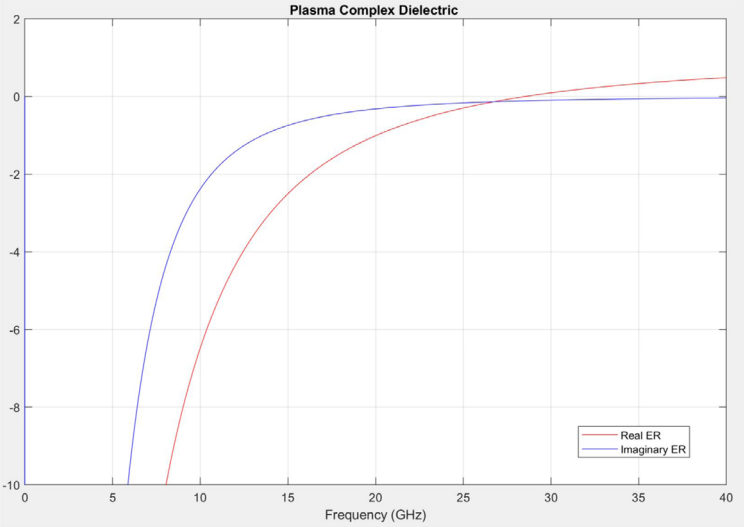

Figure 1: Real and Imaginary parts of the permittivity of the example plasma material defined in [5].

3. Validations for One-Dimensional Cases

The plasma model developed for use in XFdtd in the previous section will be validated for a series of one-dimensional cases by comparison to analytical solutions.

3.1 Normal Incidence on Plasma Half-Space

First, consider a plasma half-space with normal incidence scattering as shown in Figure 2. This interface is illuminated by a normal incident (to the interface) perpendicularly polarized plane wave traveling in the +z direction. The incident electric field, Ey, is parallel to the interface or *perpendicular* to the plane shown in Figure 2. If the following conditions hold true

$$\mu_1 = \mu_0$$

$$\varepsilon_1 = \varepsilon_0 \varepsilon_r$$

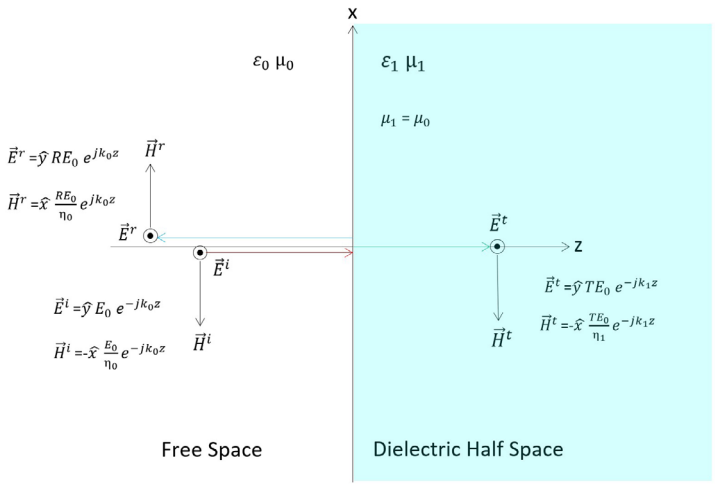

Figure 2: One dimensional geometry of plasma half-space with incident, reflected, and transmitted fields shown.

then the reflection and transmission coefficients reduce to

$$R = \frac{1 - \sqrt{\varepsilon_r}}{1 + \sqrt{\varepsilon_r}}$$

$$T = \frac{2}{1 + \sqrt{\varepsilon_r}}$$

At the air-plasma interface (z =0) the incident and reflected electric fields are

$$E_i = E_0$$

$$E_r = RE_0$$

Therefore, the ratio of the reflected and incident fields is

$$\frac{E_r}{E_i} = R$$

This value is often described in decibels as the return loss by taking the logarithm of the ratio

$$Return\ Loss = 10log_{10}\left|R^2\right|$$

The transmission (as referenced to the incident field) into the plasma at a specific distance from the interface can be found similarly with a ratio of the incident and transmitted fields.

The incident field (at the air-plasma interface, i.e. z = 0) and the transmitted field into the plasma (at some distance, z) are

$$E_i = E_0$$

$$E_t = T\,E_0\,e^{-jk_0\sqrt{e_r}z}$$

Therefore, the ratio of the transmitted and incident fields is

$$\frac{E_t}{E_i} = T\,e^{-jk_0\sqrt{e_r}z}$$

At z = 0.1 m

$$\frac{E_t}{E_i} = T\,e^{-jk_0\sqrt{e_r}(0.1)}$$

The following equation is the expression of field transmission in dB into the plasma at a distance of 0.1 m

$$Transmission = 10log_{10}\left|\left(Te^{-jk_0\sqrt{e_r}(0.1)}\right)^2\right|$$

This one-dimensional propagation case was replicated in XFdtd by creating a rectangular block of the plasma material with periodic boundaries on the (+/-) x and y directions and an absorbing boundary on the +z side. The plasma material is defined using the Debye-Drude description mentioned previously from [5]. A plane wave excitation with a broadband pulse is applied from the -z direction. The resulting reflection coefficient and transmission at a point 0.1 meters into the plasma are plotted in Figure 3 where the analytical solution is compared to those from XFdtd for the reflection. For the transmission, it can be seen that below -120 dB the computational solution is limited by the very low signal level and numerical noise.

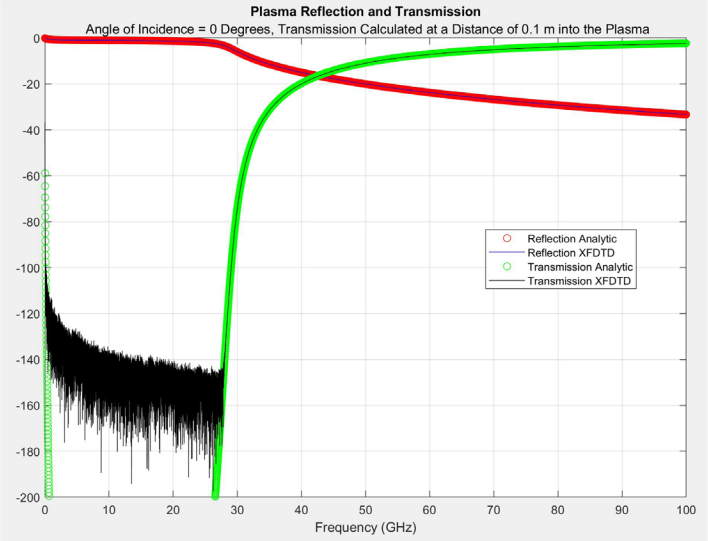

Figure 3: Reflection and Transmission at 0.1 m distance from the plasma half-space interface of Figure2, computed analytically and simulated with XFdtd.

3.2 Normal Incidence on Plasma of Finite Thickness

In this section, consider the reflection and transmission of a plane wave which is normally incident on a sheet of plasma of finite thickness such as shown in Figure 4. The analytic formulation employs the wave-transmission (wave-chain) matrix approach as outlined in Field Theory of Guided Waves by R. E. Collin [6]. This approach assumes only forward and backward TEM traveling waves and that the sections between the discontinuities (dielectric interfaces) are sufficiently long so that there is no interaction between evanescent waves generated at one interface and the adjacent interfaces.

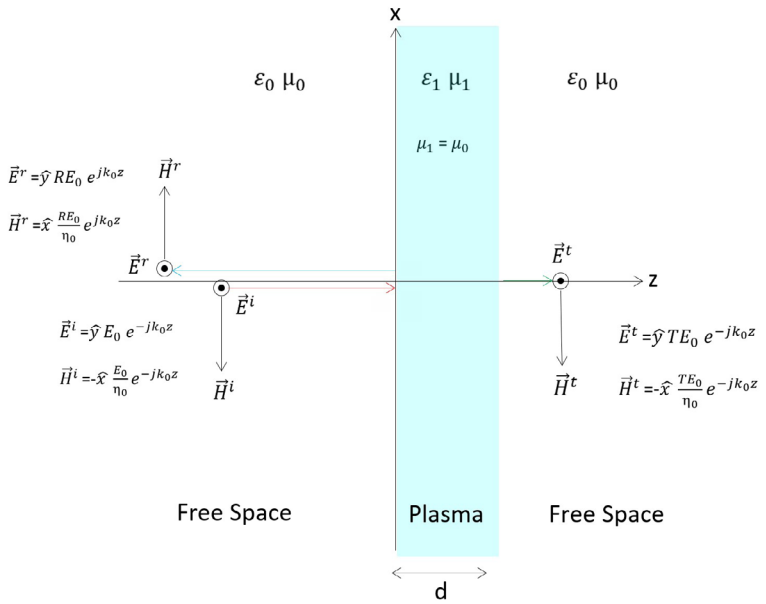

Figure 4: One Dimensional geometry of finite thickness plasma in free space with incident, reflected, and transmitted fields.

At each interface there exists a reflection and transmission coefficient as shown in Figure 5. Each interface has forward and backward propagating signals which are detailed in Figure 6. The signals a_1 and b_1 at the left of the first interface may be described by the following expressions.

$$\begin{bmatrix} a_1 \\ b_1 \end{bmatrix} = \frac{1}{T_1 T_2} \begin{bmatrix} e^{jk_1 t} & R_1 e^{-jk_1 t} \\ R_1 e^{jk_1 t} & e^{-jk_1 t} \end{bmatrix} \begin{bmatrix} 1 & R_2 \\ R_2 & 1 \end{bmatrix} \begin{bmatrix} a_3 \\ 0 \end{bmatrix}$$

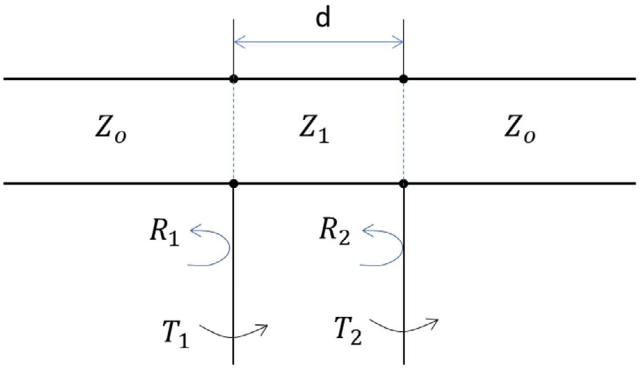

Figure 5: Diagram of the Equivalent Circuit for Plane Wave Scattering from a sheet of dielectric (thickness d) depicting the associated reflection and transmission coefficients.

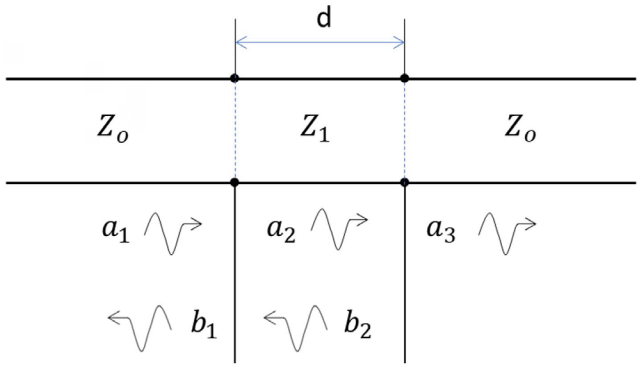

Figure 6: Diagram of the equivalent circuit for plane wave scattering from a sheet of dielectric (thickness d) depicting the traveling waves in each region.

The total or combined reflection coefficient for net impact of interactions with both interfaces of the plasma layer at the first air-plasma interface (Z=0 in Figure 4) can be found using the above matrix equation and written as the ratio of the forward traveling wave, a_1 to the reflected wave, b_1.

$$R = \frac{b_1}{a_1} = \frac{R_1 e^{jk_1 t} + R_2 e^{-jk_1 t}}{e^{jk_1 t} + R_1 R_2 e^{-jk_1 t}}$$

Likewise for the transmission coefficient relating the incident right traveling wave to the right traveling wave in the free space region on the back side of the plasma sheet, the ratio of a_3 to a_1 may be written as

$$T = \frac{a_3}{a_1} = \frac{T_1 T_2}{e^{jk_1 t} + R_1 R_2 e^{-jk_1 t}}$$

Using the same plasma material from the half-space validation, the reflection and transmission coefficients are computed analytically and simulated in XFdtd and are shown in Figure 7 for a case where the plasma layer is 1 mm thick. Very good agreement between the XFdtd method and the analytical solutions is found.

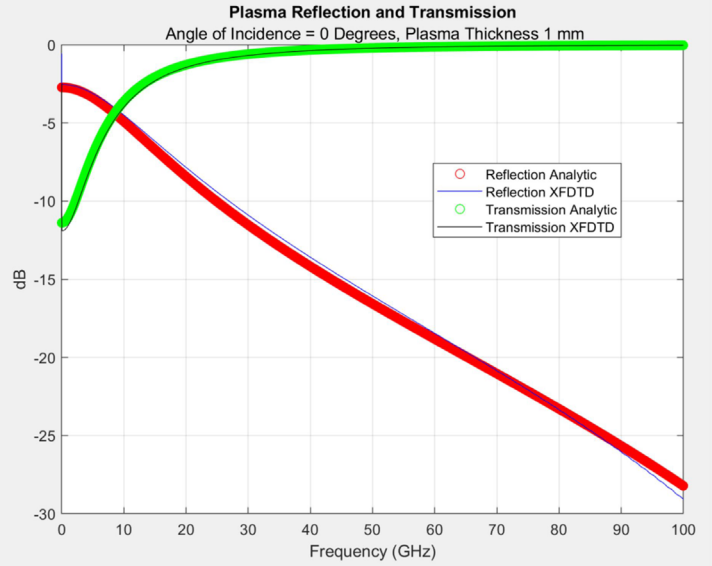

Figure 7: The reflection and transmission coefficients for a 1 mm thick plasma layer computed analytically and with XFdtd.

3.3 Normal Incidence on a Finite Thickness Plasma Sheet over PEC Half-Space

As the next one-dimensional validation, consider a thin layer of plasma material backed by a perfectly-conducting (PEC) half-space as shown in Figure 8. Here there will be an incident field from the -Z direction, a transmitted field into the plasma layer, a reflected field from the free space-plasma interface, and a second reflected field from the plasma-PEC interface.

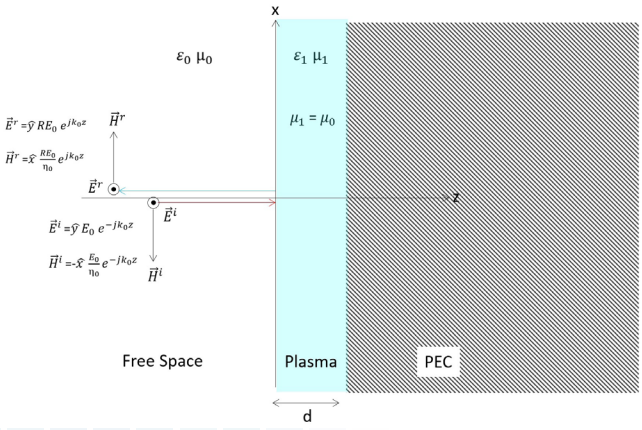

Figure 8: One-dimensional geometry of a thin plasma layer backed by a conducting half-space with incident and reflected fields shown.

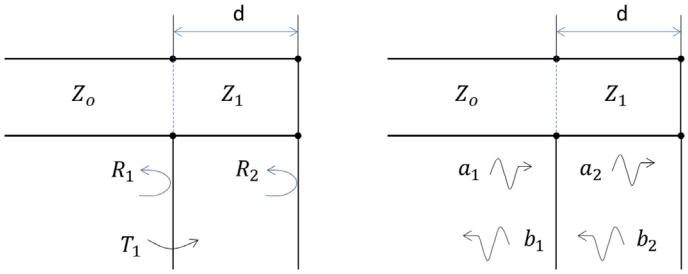

Figure 9: Interactions with the two material interfaces are shown with definitions of the various coefficients and signals.

The interactions with the two interfaces are shown in Figure 9 where two reflection terms and one transmission term are defined for signals at both interfaces. The equations for the fields may be written with the understanding that the PEC block will completely reflect any incoming signal.

$$\begin{bmatrix} a_1 \\ b_1 \end{bmatrix} = \frac{1}{T_1} \begin{bmatrix} e^{jk_1 d} & R_1 e^{-jk_1 d} \\ R_1 e^{jk_1 d} & e^{-jk_1 d} \end{bmatrix} \begin{bmatrix} a_2 \\ b_2 \end{bmatrix}$$

$$b_2 = -a_2$$

The reflection coefficient for the entire geometry is then computed as the ratio of the signals b_1 and a_1. This may be written as

$$R = \frac{b_1}{a_1} = \frac{R_1 e^{jk_1 d} - e^{-jk_1 d}}{e^{jk_1 d} - R_1 e^{-jk_1 d}}$$

The reflection computed using this equation is compared to XFdtd simulated results for a plasma layer using the same material parameters as the other cases, but here with a varying thickness. The following plasma/PEC configurations were considered for analytic and XFdtd analysis. For the case of a 1 mm thick plasma layer, the layer is too thin to cause significant interactions of the forward and backward signals and the result is a relatively smooth plot, as shown in Figure 10. When the thickness of the plasma layer is increased to 10 mm, some nulls appear in the reflection from internal reflections, as shown in Figure 11. Finally, at a plasma thickness of 50 mm, there are many interactions resulting in a response with many nulls, as shown in Figure 12. In all cases, the XFdtd results are a close match to the analytical solutions.

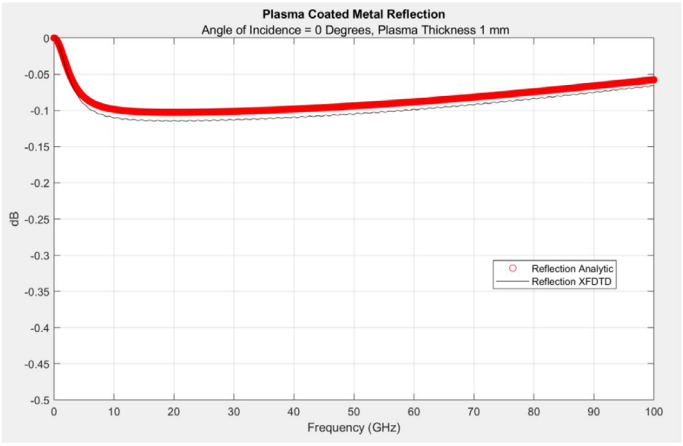

Figure 10: Reflection coefficient comparison for a plasma layer of 1 mm thickness backed by a PEC block. The layer is thin and results in a slight attenuation in the reflection.

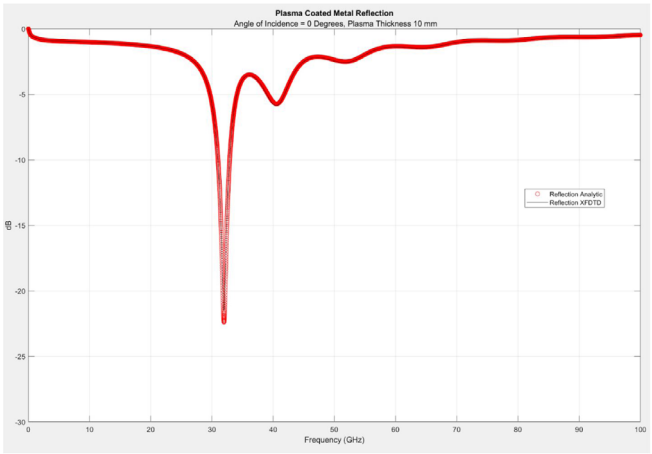

Figure 11: Reflection coefficient comparison for a plasma layer of 10 mm thickness backed by a PEC block. The layer thickness is large enough to cause a deep null in the response.

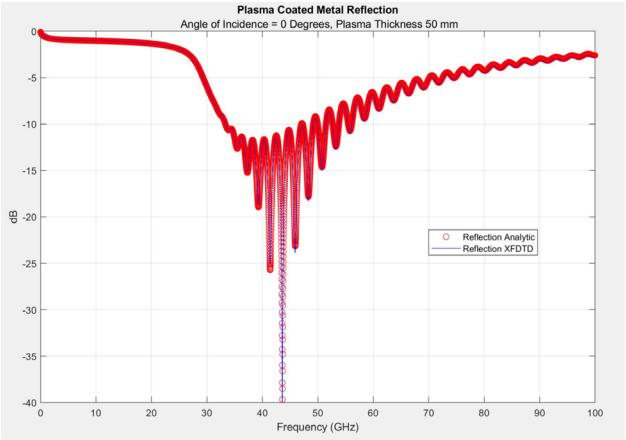

Figure 12: Reflection coefficient comparison for a plasma layer of 50 mm thickness backed by a PEC block. Here the thick plasma layer causes a more complex response; there is good agreement between XFdtd and the analytical solution.

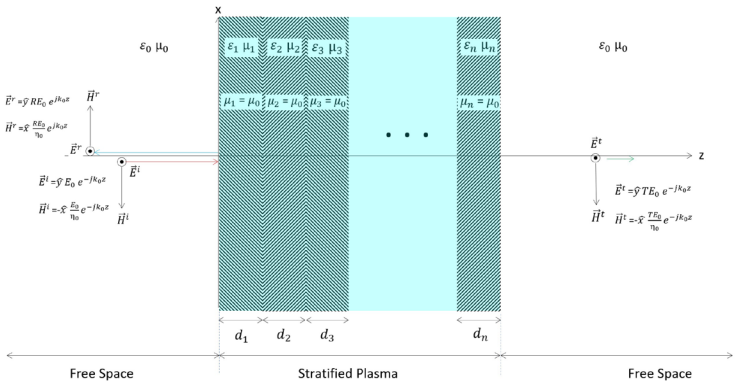

Figure 13: The one-dimensional layout of stratified media with multiple plasma layers is shown with the incident, reflected, and transmitted fields detailed.

3.4 Normal Incidence on Stratified Plasma

A final one-dimensional case to consider is normal incidence scattering on stratified plasma, as shown in Figure 13 where numerous layers of material are shown with the associated fields. Here the incident field will interact with each layer producing many internal reflections in the plasma and generating a complex reflection response.

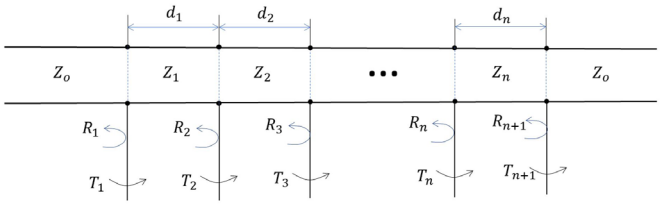

Figure 14: The equivalent circuit model for the stratified layer geometry has reflection and transmission coefficients at each interface.

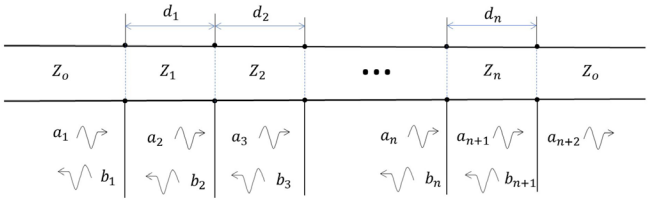

Figure 15: The traveling wave representation of the stratified plasma geometry is shown to define the various forward and backward traveling waves at each layer interface.

To compute the analytical solution for the stratified plasma case, consider the equivalent circuit diagram shown in Figure 14 where a reflection and transmission coefficient are generated at each boundary. The signals created are represented in Figure 15 where each boundary has a reflected "a" component and a transmitted "b" component. Since there is no reflection once the wave penetrates through the last plasma layer (i.e., layer n) the cascaded wave-transmission (wave-chain) matrix becomes

$$\begin{bmatrix} a_1 \\ b_1 \end{bmatrix} = \left[\prod_{i=1}^{n} \frac{1}{T_i} \begin{bmatrix} e^{jk_i d_i} & R_i e^{-jk_i d_i} \\ R_i e^{jk_i d_i} & e^{-jk_i d_i} \end{bmatrix} \right] \frac{1}{T_{n+1}} \begin{bmatrix} 1 & R_{n+1} \\ R_{n+1} & 1 \end{bmatrix} \begin{bmatrix} a_{n+2} \\ 0 \end{bmatrix}$$

The reflection and transmission coefficients at each respective dielectric interface are as defined previously for a single layer plasma. The reflection and transmission of the overall stratified media configuration is given as

$$R = \frac{b_1}{a_1}$$

$$T = \frac{a_{n+2}}{a_1}$$

The values in the equation are taken from the signals shown in Figure 15.

For an example simulation, the plasma layer is broken into six layers with constant electron densities for each step as shown in Figure 16 (after [7]). The parameters for the Debye-Drude equation are then computed at the center point for each of the six layers which are 10 mm thick. The parameters used are shown in the table of Figure 17 and the resulting geometry of six plasma layers with an incident plane wave is shown in Figure 18.

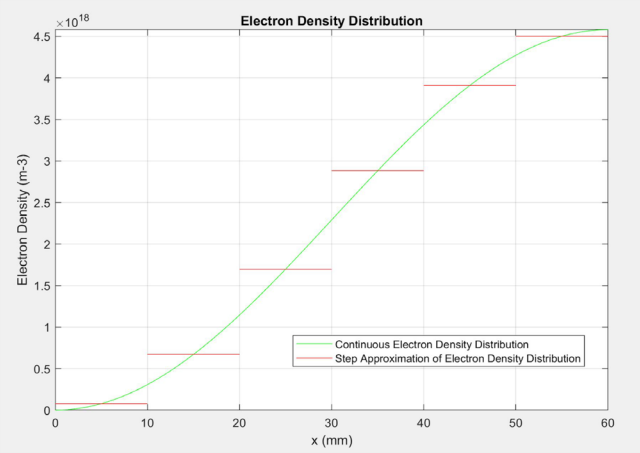

Figure 16: For the demonstration, a continuous electron density distribution is broken into six discrete steps to represent the plasma layers.

Electron Density (m-3)	7.8030E+16	6.7073E+17	1.6973E+18	2.8827E+18	3.9093E+18	4.5020E+18
Spatial Extent (mm)	0 - 10	10 - 20	20 - 30	30 - 40	40 - 50	50 -60
Plasma Frequency (GHz)	2.5046	7.3432	11.6813	15.2234	17.728	19.0245
Collision Frequency (GHz)	20	20	20	20	20	20
Eplison at Infinity	1	1	1	1	1	1
Static Eplison	0.3808776275	-4.321945945	-12.46734856	-21.87299647	-30.01838852	-34.72121715
Plasma Conductivity Sigma (S/m)	1.10E-01	9.42E-01	2.38E+00	4.05E+00	5.49E+00	6.33E+00
Relaxation Time (second)	50.0E-12	50.0E-12	50.0E-12	50.0E-12	50.0E-12	50.0E-12

Figure 17: The parameters for each of the six layers of the plasma material for use in the Debye-Drude equation are defined for each of the 10mm thick layers.

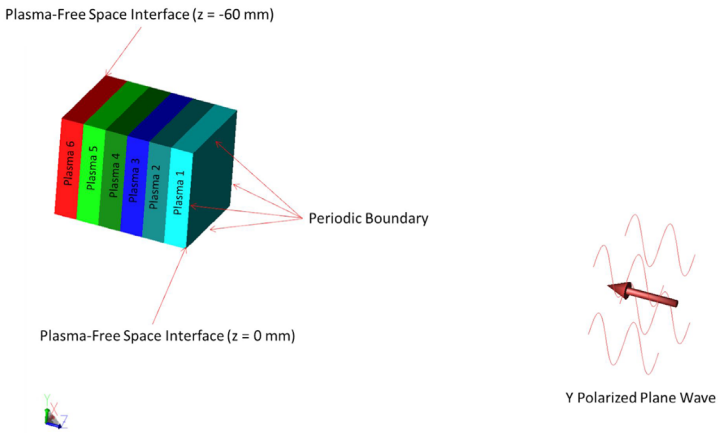

Figure 18: The geometry simulated is shown with an incident plane wave on the six-layer structure bounded by periodic boundary conditions on the four edges.

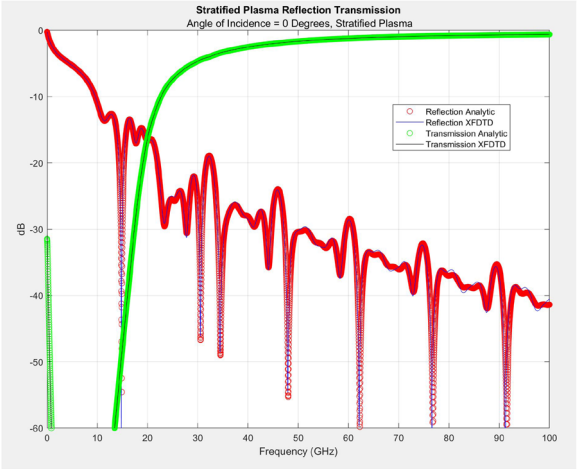

Figure 19: The resulting reflection and transmission coefficients from the six-layer plasma structure show a complex reflection profile with nulls produced from the wave interactions at the various layers. The results between the analytical and the XFdtd simulation are very similar.

The reflection and transmission coefficients are computed and the geometry is simulated in XFdtd to produce the plot shown in Figure 19. It can be seen in Figure 19 that the response is complex with multiple nulls from interactions at the various material boundaries. The XFdtd and analytical results are very similar across the frequency range.

4. Validation of Three-Dimensional Plasma Simulations

In three dimensions, validations to analytical solutions become significantly more complex. Extensive work has been performed to compute the scattering from homogeneous spherical objects, generally referred to as the Mie Solution, such as in electromagnetic textbooks like [8] and papers such as [9]. For inhomogeneous spheres, such as spheres coated by dielectric materials, the computations are more complex but have been computed in papers such as [9], [10], and [11]. Bistatic scattering from radially inhomogeneous spheres may be computed using approaches such as those in [12] or [9]. These methods involve a great deal of advanced mathematics and are best understood by reviewing the original source material as the explanations are too extensive for this paper.

In this section, Radar Cross Section (RCS) calculations of three-dimensional spheres will be compared to simulated results for the cases of a perfectly conducting metal sphere, a solid plasma sphere, and a PEC sphere coated with a thin layer of plasma material.

4.1 PEC Sphere Scattering – Monostatic

Monostatic RCS from a sphere is typically defined by three different operating regions which depend on the electrical size of the sphere. At frequencies where the sphere appears very small compared to the wavelength of the incident field, the RCS response increases by the 4th power of ka (where k is the free space wavenumber and a is the radius of the sphere) as the wavelength gets smaller; this region is defined as the Rayleigh Region where ka < 1 [13].

As the sphere size approaches approximately ten percent of the wavelength of the incident field, the RCS response becomes more complex, as there are strong contributions from both the specular reflections from the front of the sphere and from fields that wrap around (or creep) behind the sphere and are radiated off. This is referred to as the Mie Region where there is a complex ringing response in the RCS as the contributions from the creeping waves add both constructively and destructively.

Finally, when the sphere becomes very large compared to the incident wavelength, the response flattens out to a constant value and is said to have entered the Optical Region. The RCS response as a function of the normalized sphere circumference divided by the wavelength is shown in Figure 20, where the three regions are labeled and results from the analytical solutions and XFdtd are plotted. The analytical results are computed using (equation 7-12 from [9])

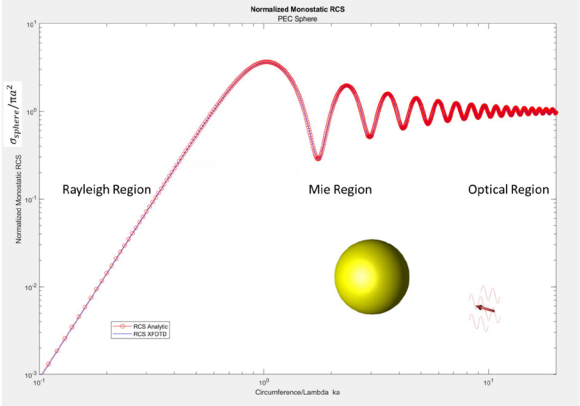

Figure 20: The normalized monostatic RCS of a perfectly conducting sphere is shown on a logarithmic scale with the three primary regions of response detailed. The XFdtd simulations are a very good match to the analytic results.

$$\bar{\gamma}(\theta=0,\phi=0) = je^{-jk_0 r}\frac{\sqrt{\pi}}{k_0}\sum_{n=1}^{\infty}(-1)^n(2n+1)\left(-\frac{j_n(k_0a)}{h_n^{(2)}(k_0a)}+\frac{j_n(k_0a)+k_0aj_n'(k_0a)}{h_n^{(2)}(k_0a)+k_0ah_n^{(2)\prime}(k_0a)}\right)\left(\frac{\hat{x}\pm j\hat{y}}{\sqrt{2}}\right)$$

The RCS is computed as

$$\sigma_{\hat{e}_{rx}} = |\vec{\gamma}(\theta,\phi)\cdot\hat{e}_{rx}|^2$$

where the three terms are defined as

$$Normalized\ Complex\ Vector\ Scattering\ Length = \vec{\gamma}(\theta,\phi)$$
$$Radar\ Cross\ Section = \sigma_{\hat{e}_{rx}}$$
$$Received\ Polarization\ Unit\ Vector = \hat{e}_{rx}$$

4.2 Plasma Sphere Scattering – Monostatic

Replacing the PEC sphere with a dielectric sphere introduces characteristics to the RCS response since the incident field will be able to penetrate the sphere and possibly create reflecting fields that will add to the complexity of the response. As is demonstrated in [9], a lossless dielectric can have a very complex response due to resonances in the sphere which are undampened. Adding loss to the dielectric reduces the complex interactions, but the RCS response will still be more complex than that of the PEC sphere.

The analytical response is computed using equation 7-15 from [9] which defines the vector scattering length as

$$\bar{\gamma}(\theta,\phi) = E_0 j \left(\frac{\hat{x} \pm j\hat{y}}{\sqrt{2}}\right)\frac{\sqrt{\pi}}{k}\sum_{n=1}^{\infty}(-1)^n\,(2n+1)\left(\frac{j_n(k_0a)\sqrt{\frac{\epsilon\mu_0}{\mu\epsilon_0}}\frac{1}{ka}\frac{\partial}{\partial a}(aj_n(ka)) - j_n(ka)\frac{1}{ka}\frac{\partial}{\partial a}(aj_n(ka))}{j_n(ka)\frac{1}{ka}\frac{\partial}{\partial a}\left(ah_n^{(2)}(k_0a)\right) - \sqrt{\frac{\epsilon\mu_0}{\mu\epsilon_0}}h_n^{(2)}(k_0a)\frac{1}{ka}\frac{\partial}{\partial a}(aj_n(ka))} + \frac{j_n(k_0a)\frac{1}{ka}\frac{\partial}{\partial a}(aj_n(ka)) - \sqrt{\frac{\epsilon\mu_0}{\mu\epsilon_0}}j_n(ka)\frac{1}{ka}\frac{\partial}{\partial a}(aj_n(k_0a))}{h_n^{(2)}(k_0a)\frac{1}{ka}\frac{\partial}{\partial a}(aj_n(ka)) - \sqrt{\frac{\epsilon\mu_0}{\mu\epsilon_0}}j_n(ka)\frac{1}{ka}\frac{\partial}{\partial a}\left(ah_n^{(2)}(k_0a)\right)}\right)$$

The RCS is computed from the vector scattering length in a manner like that used in the PEC sphere case from section 4.1.

For this demonstration, the sphere will have a radius of 10 mm and be assigned the material properties of the plasma used previously for the one-dimensional cases (that from [5]). The analytical and XFdtd simulated results for the monostatic RCS are plotted in Figure 21. Note that the XFdtd and analytical results are identical over the frequency range of 0 to 60 GHz.

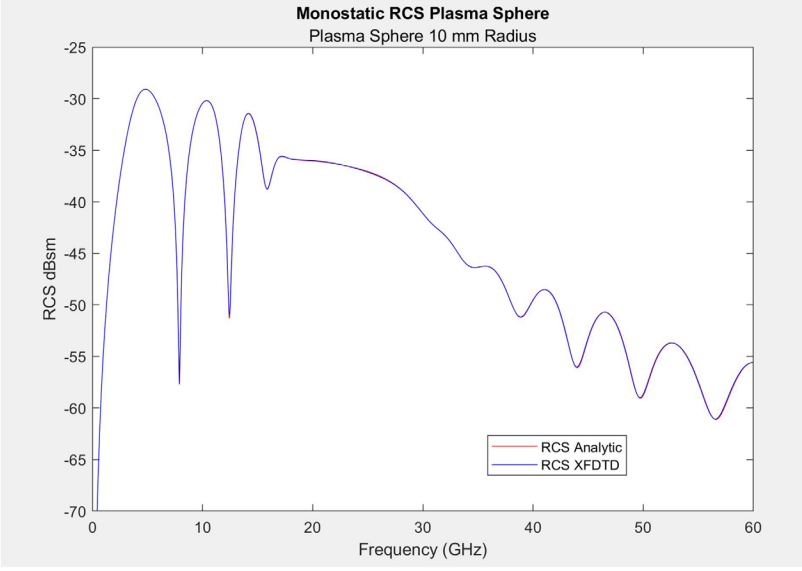

Figure 21: Monostatic RCS result comparing the analytical solution to XFdtd for a 10mm radius plasma sphere.

4.3 Plasma Coated PEC Sphere – Monostatic

The addition of a plasma coating on a PEC sphere modifies the response in several ways, including changing the medium of the creeping waves wrapping around the sphere and the possibility of internally-reflected (internal resonances) waves inside the plasma layer. The analytical solution for the RCS from a dielectrically coated conducting sphere used here is from [11]. The solution in [11] describes the structure as a conducting sphere with radius "b" and a lossy layer with thickness "d", resulting in a total radius or "a" where a=b+d. As such, the scattering cross section is then given in [11] as

$$\frac{\sigma}{\pi a^2} = \frac{1}{(k_0 a)^2}\left|\sum_{n=1}^{\infty}(-1)^n(2n+1)\left(a_n^{TE} - b_n^{TM}\right)\right|^2$$

where the various terms are defined as

$$a_n^{TE} = -\frac{k_0 a j_n(k_0 a) - jZ_n[k_0 a j_n(k_0 a)]'}{k_0 a h_n(k_0 a) - jZ_n[k_0 a h_n(k_0 a)]'}$$

$$b_n^{TM} = -\frac{k_0 a j_n(k_0 a) - jY_n[k_0 a j_n(k_0 a)]'}{k_0 a h_n(k_0 a) - jY_n[k_0 a h_n(k_0 a)]'}$$

$$jZ_n = \frac{1}{\sqrt{\varepsilon_r}}\left[\frac{k_0\sqrt{\varepsilon_r}a j_n\left(k_0\sqrt{\varepsilon_r}a\right) - \frac{j_n\left(k_0\sqrt{\varepsilon_r}b\right)}{h_n\left(k_0\sqrt{\varepsilon_r}b\right)}k_0\sqrt{\varepsilon_r}a h_n\left(k_0\sqrt{\varepsilon_r}a\right)}{\left[k_0\sqrt{\varepsilon_r}a j_n\left(k_0\sqrt{\varepsilon_r}a\right)\right]' - \frac{j_n\left(k_0\sqrt{\varepsilon_r}b\right)}{h_n\left(k_0\sqrt{\varepsilon_r}b\right)}\left[k_0\sqrt{\varepsilon_r}a h_n\left(k_0\sqrt{\varepsilon_r}a\right)\right]'}\right]$$

and

$$jY_n = \sqrt{\varepsilon_r}\left[\frac{k_0\sqrt{\varepsilon_r}a j_n\left(k_0\sqrt{\varepsilon_r}a\right) - \frac{\left[k_0\sqrt{\varepsilon_r}b j_n\left(k_0\sqrt{\varepsilon_r}b\right)\right]'}{\left[k_0\sqrt{\varepsilon_r}b h_n\left(k_0\sqrt{\varepsilon_r}b\right)\right]'}k_0\sqrt{\varepsilon_r}a h_n\left(k_0\sqrt{\varepsilon_r}a\right)}{\left[k_0\sqrt{\varepsilon_r}a j_n\left(k_0\sqrt{\varepsilon_r}a\right)\right]' - \frac{\left[k_0\sqrt{\varepsilon_r}b j_n\left(k_0\sqrt{\varepsilon_r}b\right)\right]'}{\left[k_0\sqrt{\varepsilon_r}b h_n\left(k_0\sqrt{\varepsilon_r}b\right)\right]'}\left[k_0\sqrt{\varepsilon_r}a h_n\left(k_0\sqrt{\varepsilon_r}a\right)\right]'}\right]$$

For a test problem, consider a PEC sphere with radius 100 mm covered by a plasma layer of 10 mm thickness, as shown in Figure 22. The plasma layer will be defined using the parameters from [5]. The monostatic RCS over a frequency range of 0 to 20 GHz is plotted in Figure 23 and shows excellent agreement between XFdtd and the analytical solution at frequencies below 12 GHz and has good but slightly varying results in the optical range above 12 GHz.

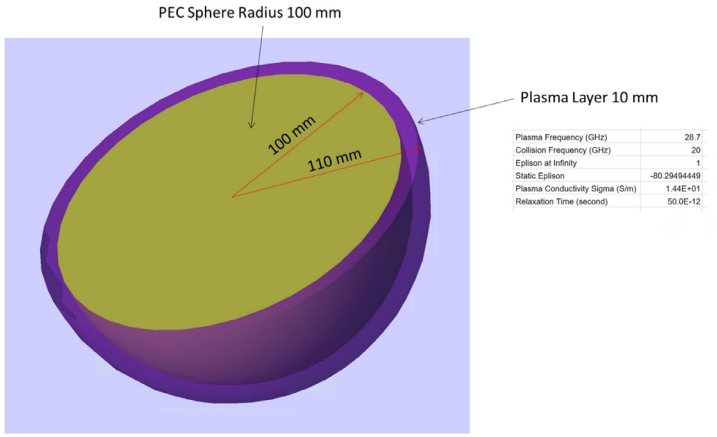

Figure 22: Cut-away view of the PEC sphere of radius 100 mm coated by a 10 mm thick layer of plasma material.

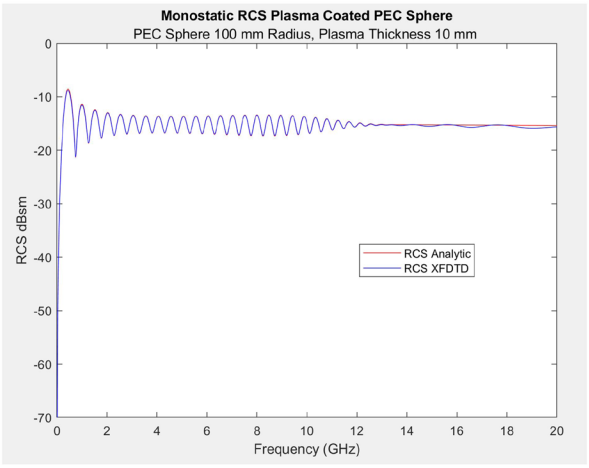

Figure 23: Monostatic RCS of 100 mm radius PEC sphere coated with 10 mm thick layer of plasma.

4.4 Plasma Coated PEC Sphere – Bistatic

The previous examples showed monostatic RCS results versus frequency, but another result of interest is the bistatic scattering at a single frequency. First consider a plasma coated PEC sphere like that used in section 4.3 with an inner radius of "b", an outer radius of "a", and a plasma thickness of "d". The plasma coated PEC sphere bistatic RCS formulation employs the coefficients of the TE and TM modes found in section 4.3 for the monostatic RCS analytic formulation and radially independent vector spherical harmonic functions. The TE and TM coefficients of coated metal spheres can be found in [11] while the spherical harmonics details are provided in [12].

The TE and TM mode coefficients for scattering from a plasma coated PEC sphere were described in section 4.3 at the values a_n^{TE} and b_n^{TM}. For the spherical harmonics, their formulation assumes the incident plane wave is X polarized and is traveling from the -Z direction. They can be written as

$$P(\theta) = \sum_{n=1}^{\infty} \frac{2n+1}{n(n+1)} \left[a_n^{TE} \frac{d}{d\theta} P_n^1(cos\theta) + b_n^{TM} \frac{P_n^1(cos\theta)}{sin\theta} \right]$$

$$Q(\theta) = \sum_{n=1}^{\infty} \frac{2n+1}{n(n+1)} \left[a_n^{TE} \frac{P_n^1(cos\theta)}{sin\theta} + b_n^{TM} \frac{d}{d\theta} P_n^1(cos\theta) \right]$$

$P_n^1(cos\theta)$ *is the associated Legendre function* of order n and index 1

The E- Plane bistatic RCS is given by the following equation

$$\sigma_e(\theta) = \frac{4\pi}{k_0^2}|P(\theta)|^2$$

The H-Plane bistatic RCS is given by the following equation

$$\sigma_h(\theta) = \frac{4\pi}{k_0^2}|Q(\theta)|^2$$

Using these equations on the test geometry of Figure 22 of a 100 mm radius PEC sphere with a 10 mm plasma coating (plasma properties as described in [5]), the bistatic RCS in the E- and H-Planes may be computed and compared to results from XFdtd. The bistatic results at frequencies of 2, 3, 4, and 5 GHz are shown in Figure 24 through Figure 27. The XFdtd results show excellent agreement with the Analytic solution for all frequencies.

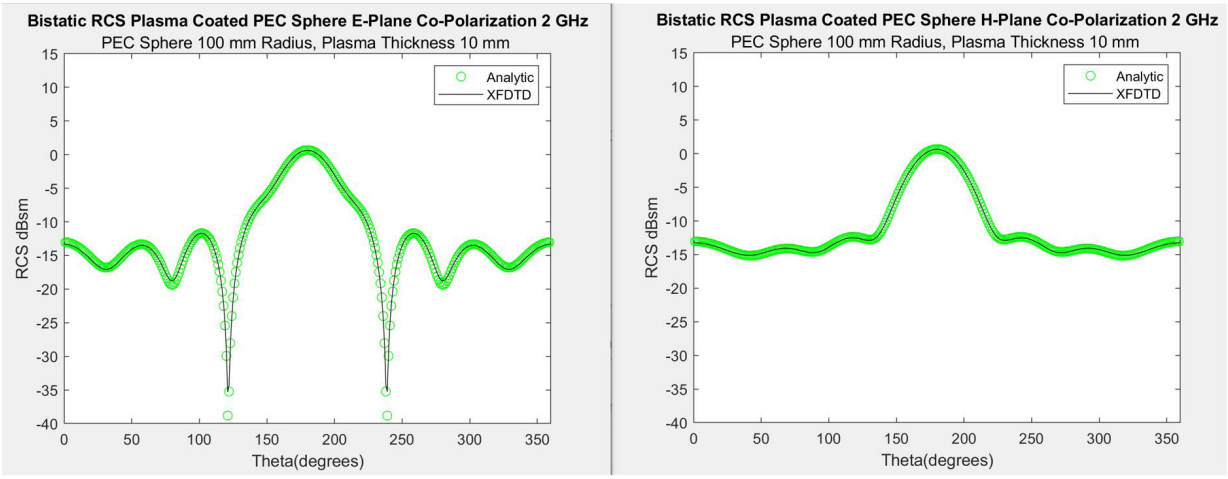

Figure 24: Bistatic RCS results for the plasma coated sphere at 2 GHz in the E-Plane (left) and H-Plane (right). The XFdtd results show excellent agreement with the Analytic solution.

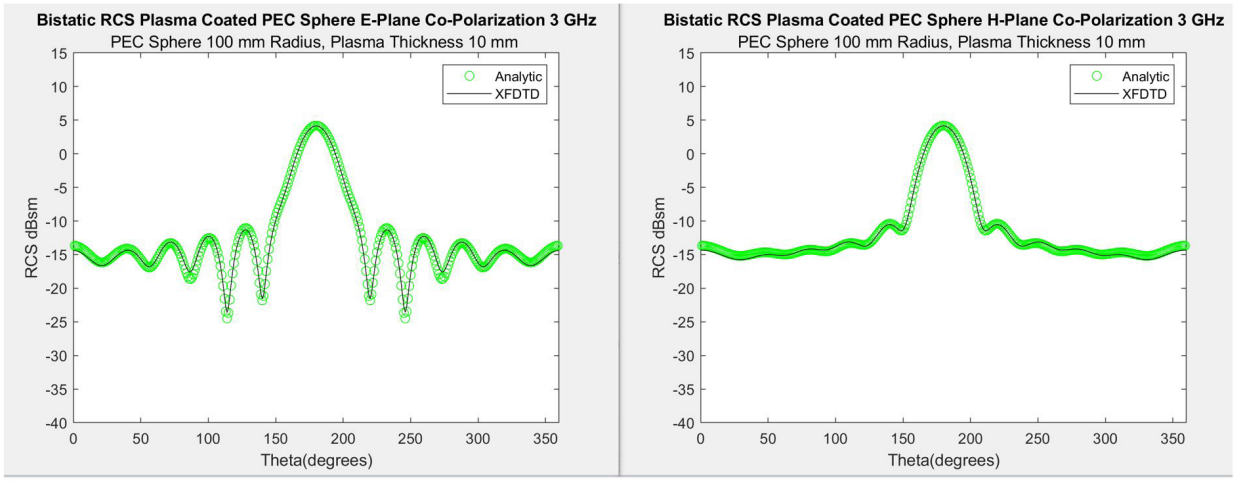

Figure 25: Bistatic RCS results for the plasma coated sphere at 3 GHz in the E-Plane (left) and H-Plane (right).

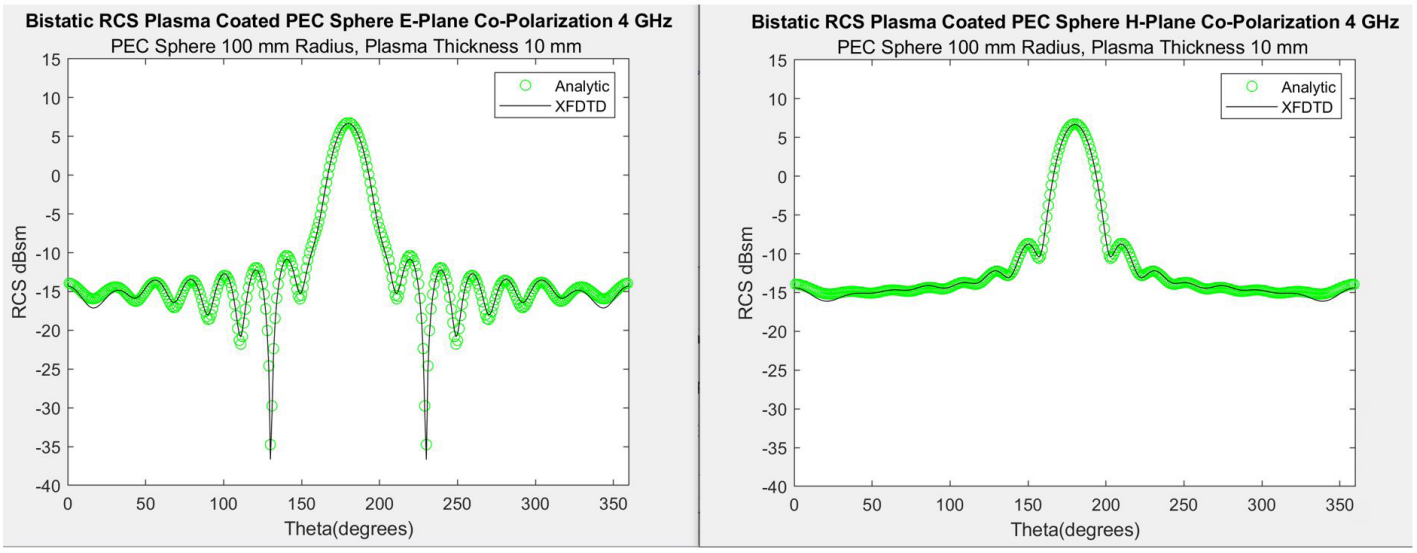

Figure 26: Bistatic RCS results for the plasma coated sphere at 4 GHz in the E-Plane (left) and H-Plane (right).

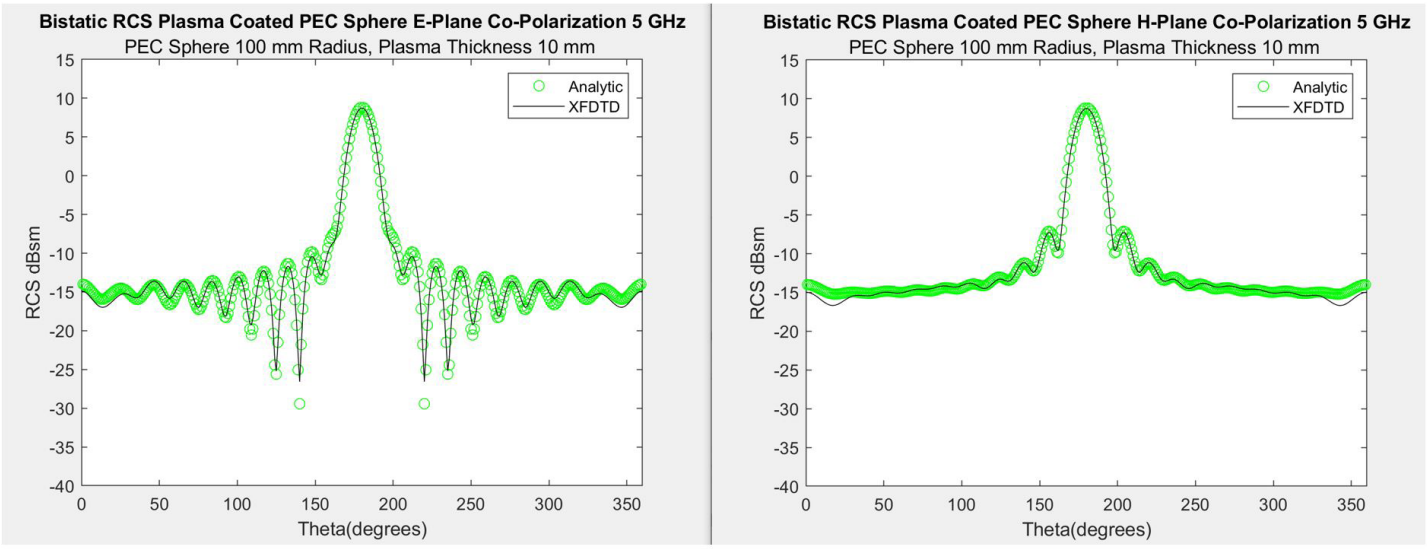

Figure 27: Bistatic RCS results for the plasma coated sphere at 5 GHz in the E-Plane (left) and H-Plane (right).

4.5 PEC Sphere – Bistatic RCS

The bistatic scattering from a PEC sphere may be computed analytically using the same equations as in section 4.4 and simply setting the dielectric constant of the plasma layer to free space. Repeating the simulations for the plasma-coated sphere for only the PEC core gives results as shown in Figure 28 at 2 GHz, where the XFdtd results are a perfect match to the Analytic solution.

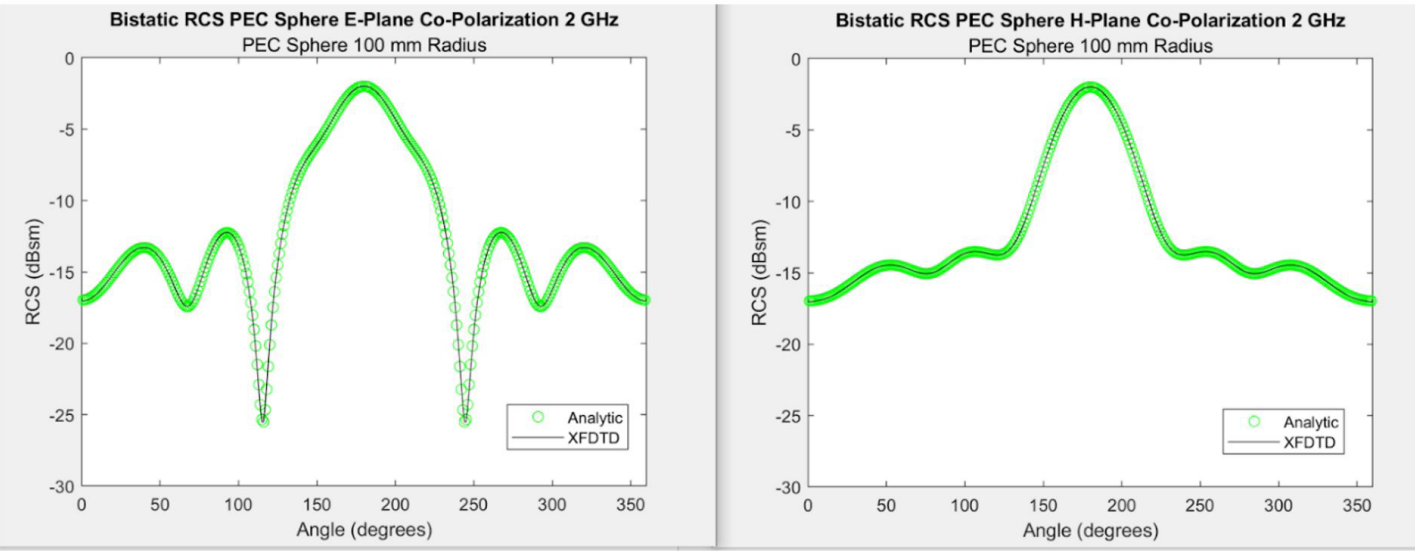

Figure 28: Bistatic RCS results for a 100 mm radius PEC sphere in the E-Plane (left) and H-Plane (right).

5. Conclusion

Analytic solutions to one-dimensional interactions of incident waves on various planar surfaces were developed and compared to XFdtd with excellent agreement found. Examples of plasma half-planes, finite thickness plasma layers, plasma-coated PEC half-planes, and stratified plasma layers were examined. In three dimensions, solutions were derived for PEC spheres, plasma spheres, and plasma coated PEC spheres. Both monostatic and bistatic RCS results were shown with good agreement between the analytic and XFdtd computational solutions. These results give confidence that XFdtd may be used for more complex structures for which analytic solutions are not readily available.

References

[1] R. Luebbers, F. P. Hunsberger, K. S. Kunz, R. B. Standler and M. Schneider, “A frequency-dependent finite-difference time-domain formulation for dispersive materials,” in *IEEE Transactions on Electromagnetic Compatibility*, vol. 32, no. 3, pp. 222-227, Aug. 1990, doi: 10.1109/15.57116.

[2] R. J. Luebbers, F. Hunsberger and K. S. Kunz, “A frequency-dependent finite-difference time-domain formulation for transient propagation in plasma,” in *IEEE Transactions on Antennas and Propagation*, vol. 39, no. 1, pp. 29-34, Jan. 1991, doi: 10.1109/8.64431.

[3] R. J. Luebbers and F. Hunsberger, “FDTD for Nth-order dispersive media,” in *IEEE Transactions on Antennas and Propagation*, vol. 40, no. 11, pp. 1297-1301, Nov. 1992, doi: 10.1109/8.202707.

[4] F. Hunsberger, R. Luebbers and K. Kunz, “Finite-difference time-domain analysis of gyrotropic media. I. Magnetized plasma,” in *IEEE Transactions on Antennas and Propagation*, vol. 40, no. 12, pp. 1489-1495, Dec. 1992, doi: 10.1109/8.204739.

[5] R. Luebbers, D. Steich and K. Kunz, “FDTD calculation of scattering from frequency-dependent materials,” in *IEEE Transactions on Antennas and Propagation*, vol. 41, no. 9, pp. 1249-1257, Sept. 1993, doi: 10.1109/8.247751.

[6] Collin, R. E., *Field Theory of Electromagnetic Waves*, Wiley-IEEE Press, 1991.

[7] Z. Han, J. Ding, P. Chen, Z. Zhang and C. Guo, “FDTD analysis of three-dimensional target covered with inhomogeneous unmagnetized plasma,” *2010 International Conference on Microwave and Millimeter Wave Technology*, Chengdu, China, 2010, pp. 125-128, doi: 10.1109/ICMMT.2010.5525270.

[8] Stratton, J. A., *Electromagnetic Theory*. McGraw Hill, 1941.

[9] Brock, Billy C. *Bistatic and Monostatic Radar Cross Section of Radially Inhomogeneous Spheres*. United States: N. p., 2016. Web. doi:10.2172/1618259.

[10] V. H. Weston and R. Hemenger, “High frequency scattering from a coated sphere,” *J. Res. Nut. Bur. Stand.*, vol. 66D, pp. 613-619, 1962.

[11] D. J. Taylor, A. K. Jordan, P. J. Moser and H. Uberall, “Complex resonances of conducting spheres with lossy coatings,” in *IEEE Transactions on Antennas and Propagation*, vol. 38, no. 2, pp. 236-240, Feb. 1990, doi: 10.1109/8.45126.

[12] J. R. Wait and C. M. Jackson, “Calculations of the bistatic scattering cross section of a sphere with an impedance boundary condition,” Radio Sci. J, *Res. Nut. Bur. Stand./ USNC-URSI*, vol. 69D, pp. 299-314, Feb. 1965

[13] Skolnik, Merrill, *Radar Handbook Second Edition*. McGraw Hill, 1990.

Remcom, Inc.
315 S. Allen St., Suite 416
State College, PA 16801 USA

+1.888.7.REMCOM (US/CAN)
+1.814.861.1299 phone
+1.814.861.1308 fax

sales@remcom.com